Aquaculture 581 (2024) 740429

Contents lists available at ScienceDirect

Aquaculture

journal homepage: www.elsevier.com/locate/aquaculture

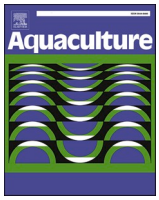

Farmed Atlantic salmon (*Salmo salar* L.) avoid intrusive objects in cages: The influence of object shape, size and colour, and fish length

Qin Zhang [a], Nina Bloecher [b], Linn Danielsen Evjemo [b], Martin Føre [a], Biao Su [b], Espen Eilertsen [b], Mats Aarsland Mulelid [b], Eleni Kelasidi [b,*]

[a] Department of Engineering Cybernetics, NTNU, 7039 Trondheim, Norway
[b] Department of Aquaculture Technology, SINTEF Ocean, 7010 Trondheim, Norway

ARTICLE INFO

Keywords:
Aquaculture
Salmo salar
Sonar data
Deep learning
Aquaculture robotics
Fish avoidance distance

ABSTRACT

Underwater vehicles and other mobile platforms are seeing increased use as tools within fish farming, particularly due to current trends towards Precision Farming practices, and more exposed farming sites. Although many of the applications of such tools (e.g., net cleaning and inspection) have become well established industrial practices, it is largely unknown how much such operations disturb the fish and the consequence of this disturbance. In this study, we explored this by exposing Atlantic salmon in commercial net cages to intrusive objects and monitoring the distribution of fish around these using on-board 360-degree sonars. Six different object designs were tested covering variations in size, shape, and colour, which are important static characteristics of underwater vehicles/platforms. The sonar data was first aggregated into images containing the Cumulative Fish Presence over 1-, 5- and 10-min periods to provide a more robust foundation for further analyses. By training a deep learning based method using UNet++ architecture to automatically segment the fish distribution patterns, the mean distance between the inner perimeter of the fish distribution and the object was assessed. Results from the study implied that fish keep greater distances to larger objects. There was, however, no clear impact of the shape. Regarding the effect of colour, fish kept greater distances to yellow than to white objects. When comparing results from tests on fish of different size, data indicate a positive linear relationship between fish weight (age) and distance to an object, that can be expressed as an avoidance distance of an average 3.8 body-lengths. Our findings provide new fundamental knowledge on the dynamics between the fish and objects such as vehicles or other mobile platforms in fish farms, and thus provides valuable insights that can be useful when designing such tools specifically for aquaculture.

1. Introduction

Aquaculture is an important source of seafood, and is likely to play an important role in serving the increased food demand that will accompany a growing world population (FAO, 2020). The Norwegian aquaculture industry is mostly focused around Atlantic salmon (*Salmo salar*) production conducted at sheltered fjord/coastal sites in floating gravity type sea cages. This industry has grown rapidly in terms of production volume and economy, and produced >1.6 million tonnes of marketable fish meat with a value of >68 billion NOK in 2021(Norwegian Directorate of Fisheries, 2021-05-27).

This growth in demand has traditionally been served by establishing new farming sites in coastal areas, providing shelter against environmental forces and proximity to established infrastructure (e.g., power and communication grids, logistics). However, due to competing claims from other industries (e.g., fisheries, tourism, shipping), such coastal sites have now become scarce. Together with the expectation that conditions further from shore are more beneficial for the fish, this has stimulated the industry to move further offshore and to more exposed locations (Bjelland et al., 2015). Since changes in the production environment also require changes in the production technology and methods applied, the aquaculture industry has thus started shifting production methods from the predominantly manual and experience based operations historically used to more objective approaches based on intelligent sensors, mathematical models, decision support systems and autonomous methods in different stages of production, as proposed by the Precision Fish Farming (PFF) concept (Føre et al., 2017; Bjelland et al., 2015; Kelasidi and Svendsen, 2022). Intelligent use of Unmanned

* Corresponding author.
E-mail address: eleni.kelasidi@sintef.no (E. Kelasidi).

https://doi.org/10.1016/j.aquaculture.2023.740429
Received 28 June 2023; Received in revised form 23 November 2023; Accepted 25 November 2023
Available online 1 December 2023

Underwater Vehicles (UUVs) is a core component in realising the aims of PFF.

UUVs have been used by different industrial segments (e.g., oil and gas, shipping and conservation/oceanography) and the military (Kelasidi et al., 2016, 2017; Sverdrup-Thygeson et al., 2017; Fossen, 2011; Paull et al., 2013) to solve several types of challenges/operations (e.g., mapping, monitoring, inspection and intervention). There are several ways in which such tools can be useful within aquaculture. For instance, UUVs equipped with cameras and sensors/instruments can be used for monitoring and inspection of fish and structural components, and can also conduct increasingly complex intervention operations, thus replacing divers and hence reducing the risk of personnel injuries (Kelasidi and Svendsen, 2022). However, UUVs used in aquaculture, such as remotely operated vehicles (ROVs), are mainly based on knowledge and technology developed by other industries such as the oil and gas sector. Unlike these other industries, aquaculture operations include live fish, meaning that UUV methods and vehicles also need take the biology into account to be applicable (Kelasidi and Svendsen, 2022). This entails that vehicles used for aquaculture operations should be designed to minimise their potential negative impact on the animals, thereby improving their compatibility with fish production. This is an exercise that requires new fundamental knowledge to identify and quantify the responses of fish when subjected to different impact factors.

While some of the factors known to affect the behaviour of farmed salmon, such as temperature, oxygen and natural light, are natural elements in the cage environment (Oppedal et al., 2011), other factors, such as anthropogenic sounds (i.e., sounds arising due to human activities), artificial light and intrusive objects, may be introduced due to the use of technological tools in the cage, including moving sensors and UUVs. Atlantic salmon have been found to have a hearing range of about 100 —380 Hz (Hawkins and Johnstone, 1978; Oxman et al., 2007), and can respond to sounds from different audio sources. For example, (Pieniazek et al., 2020; Magnhagen et al., 2017) found that noise from service vessels can lead to reduction in feeding, an effect that might also occur due to sounds emitted by actuated sensors and/or UUVs. The impact of natural or artificial light on salmon behaviour is typically expressed as a trade-off between having sufficient light to feed (Fraser and Metcalfe, 1997), and being less visible for potential predators (Juell and Fosseidengen, 2004). Light can lead to increased stress levels in salmon, and light with shorter wavelengths affect salmon more (Migaud et al., 2007). In addition, it is observed that salmon prefer slight dimmed light to bright daylight and descend or ascend in the cage accordingly (Fernö et al., 1995; Føre et al., 2018). UUVs carrying lights may perturb the lighting conditions in the cage, and could thus also have an impact on the spatial distribution (Fernö et al., 1995) and even stress levels (Migaud et al., 2007) of farmed salmon. The third factor mentioned above is intrusive objects, and is perhaps the most important to consider as a sensor or UUV deployed in a cage will immediately be perceived as such an object by the fish. In addition to detection through visual means, fish can also detect nearby objects without being in contact with them using e.g., the lateral line organ (Kryvi and Totland, 1997). Fish responses towards intrusive objects have been found to depend on the object's colour, size, shape, motion and speed (Marras and Porfiri, 2012; Kruusmaa et al., 2020). One study performed by (Marras and Porfiri, 2012) showed that zebrafish (*Danio rerio*) were more attracted to a robotic fish similar in colour and dimension to a fertile female zebrafish than elongated or monochromatic robotic fish. In a study conducted in a commercial fish farm, (Kruusmaa et al., 2020) found that it was more difficult for fish to observe a silvery robot than the yellow robot, and that the fish stayed farther away from larger objects than from smaller ones when other parameters of the objects were similar. In sum, these studies imply that the colour and size of an intrusive object are important factors determining how the fish respond to this object, and that the emission of sound and light could similarly induce attraction or avoidance in the fish.

In this study, we sought to explore how the physical properties of an intrusive object affected the responses of farmed Atlantic salmon. Several field trials were conducted in industrial-scale fish farms at SINTEF ACE (SINTEF, 2023). Avoidance distance exhibited by salmon exposed to structures of various shapes, sizes, and colours were measured. The fish were stimulated in an experimental setup where these external impact factors were varied to assess their effects. To account for how variable lighting conditions may impact the visual perception of the fish, the trials were conducted at different seasons but with the device at fixed depth, thus covering a range of natural lighting conditions (Oppedal et al., 2011). The potential fish responses were recorded using different types of echo sounders and cameras. The analyses presented in this work focus on data from two 360 degree sonars. Rather than analysing manually, we developed a Deep Learning (DL)-based method for analysing the sonar data to automatically identify fish swimming patterns and quantify fish responses. And the DL-based method has been implemented and validated on the set of data we collected, aspiring to relate fish responses to different structure appearances and sizes simultaneously. The method we have developed and results we have obtained in the study can therefore provide insight needed to develop robotic solutions better suited to a co-existence with fish in sea-cages.

2. Materials and methods

2.1. Experimental setup and data acquisition

Tests were conducted at SINTEF's industrial-scale research fish farm sites in Mid-Norway, SINTEF ACE (SINTEF, 2023), in June 2021 (P1), October 2021 (P2) and September 2022 (P3). P1 and P2 were both conducted at the fish farm site Tristeinen, while P3 was conducted at the fish farm site Korsneset. Korsneset is located within a fjord, and therefore less exposed to waves and currents than Tristeinen. Tristeinen had 8 pens, while Korsneset included 12 pens, each cage containing up to 200,000 fish of the size range 1 kg to 6 kg (see Table 1). Fish observed in the three trials originated from three commonly used genetic strains (P1: Rauma, P2: SalmoBreed, P3: MoWi). Typically, the fish are fed for several hours during the day. As feeding elicits strong reactions in fish (Føre et al., 2011) which could mask the impacts of the factors of interest, all the trials were conducted while feeding was paused. While the experimental timing for P1-P3 (June, September and October) was mostly chosen based on site availability, the large range in seasonality improved the robustness of the method as the different trials were thus conducted under variable natural light levels. All tests were conducted in normal daylight hours (i.e., between 09:00 and 17:00) to reduce the potential impact of daily variations in natural light on the perception of the fish.

A test structure was designed for these experiments consisting of a cylindrical centre structure containing three stacked cylinders with dimensions Ø18 × 15, Ø30 × 30, Ø18 × 15 cm (shown to the left in Fig. 1) designed to house the sensors and actuators used in the field trials. This centre structure was mounted inside shell structures of different shapes and colours to test for the different impact factors, as shown in Fig. 1; a small cylinder with dimensions Ø30 × 30 cm, a cube with dimensions 60 × 60 × 60 cm, and a big cylinder with dimensions Ø60 × 60 cm. Note that the small cylinder was created by covering the middle cylinder of the centre structure (to the left in Fig. 1) in fabric, and therefore has the same dimensions as the centre structure. The centre structure was equipped with two Ping360 sonars: one close to the top, placed so that the beams had a clear path through the openings at the top of the shell structures, and one on the bottom extending below the lower edge of the shell structure. To capture video footage of the fish reactions as supplementary information, the structure was in addition equipped with either i) four GoPro (Hero4) cameras in equal distance to each other, pointing outwards in four directions (P1 and P2) or ii) a stereo camera, which enabled monitoring from the surface via a live feed (P3). In all trials, the structure was placed at a water depth of 8 m using a buoy and

Table 1
Overview of fish participating in field trials and factors tested.

Trial	Location	Cage	# Fish	Fish weight [kg]	Shape x Size	Colour	Date	Impact Factors
P1	Tristeinen	1	195,000	2.5	Cube	Yellow	16-Jun 2021	FW
		8	180,000	2.6	Cube	Yellow	17-Jun 2021	FW
P2	Tristeinen	1	99,000	5.0	Cube	Yellow	18-Oct 2021	FW
P3	Korsneset	12	172,000	1.0	Cube	Yellow	7-Sep 2022	FW, SSS, SC
						White	7-Sep 2022	SSS, SC
					Small cylinder	Yellow	8-Sep 2022	SSS, SC
						White	8-Sep 2022	SSS, SC
					Big cylinder	Yellow	6-Sep 2022	SSS, SC
						White	5-Sep 2022	SSS, SC
		14	175,000	1.0	Cube	Yellow	7-Sep 2022	SSS-C, SC-C
						White	6-Sep 2022	SSS-C, SC-C
					Small cylinder	Yellow	7-Sep 2022	SSS-C, SC-C
						White	7-Sep 2022	SSS-C, SC-C
					Big cylinder	Yellow	6-Sep 2022	SSS-C, SC-C
						White	5-Sep 2022	SSS-C, SC-C

Impact factors - SSS: Structure Shape and Size; SC: Structure Colour; FW: Fish weight; -C: Cage effect.

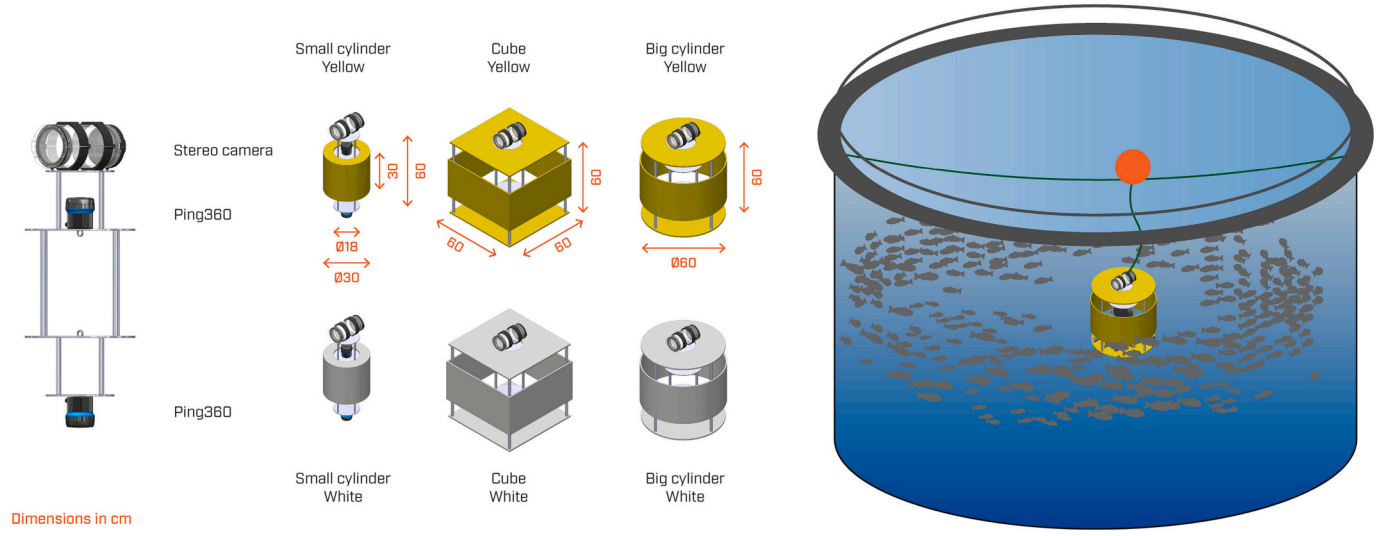

Fig. 1. Experimental setup. The centre structure (left) was equipped with a sonar on the top and on the bottom as well as either a stereo camera (on top) or four GoPro cameras (not shown), and decorated in a total of six different appearances that varied in shape, size, and colour.

ropes, as shown in Fig. 1. The choice of depth was influenced by several factors: (i) 8 m is a depth where fish are known to be present during daylight hours (Føre et al., 2018), (ii) it represents roughly the middle of the main cage volume, and thus a typical ROV operation depth, and (iii) limitation related to waterproofing of chosen equipment. To ensure comparability across the entire experiment, the structure was therefore fixed at this water depth using a buoy and ropes in all trials.

Trials conducted at the three different times tested different combinations of factors (Table 1). In P1 and P2 conducted in 2021 the rectangular yellow shell structure described as "Cube yellow" in Fig. 1 was used. The tests were conducted on fish of two different size classes (2.5–2.6 kg and 5.0 kg). In P3 conducted in 2022, all six different shell structures shown in Fig. 1 were tested on fish of 1 kg. Tests P1 and P3 were performed in 2 cages each, while P2 could only be performed in one cage. To reduce the potential impact of the fish habituating to the object and thus introducing differences between the first and last measurement in a set, the inert object was installed some time ahead of the six replicate measurements being conducted in each cage. While this might not remove potential effects due to repeated exposure, it may reduce transient effects due to completely naive fish seeing the object for the first time. A measurement consisted of a 12 min recording of fish responses, where the data recorded in the first and last minute were discarded when analysing the data. Between replicate measurements the structure was moved laterally for approx. 25 s.

The data used in the analyses was obtained using 360 degree mechanical sonars (Ping360 - Scanning Image Sonars, BlueRobotics Inc.). These sonars can be set up to acquire images at a range of up to either 5 or 10 m from the instrument. While sonar measurements obtained with a 10 m range provide data over a larger viewing area, the resolution will be lower than when set up with a 5 m range, which impacts the ability to identify and quantify fish distribution and swimming patterns. We conducted preliminary analyses to investigate this trade-off, and found that data obtained with 10 m range were too coarse to achieve the desired precision and accuracy for our study. All Ping360 data utilized in this study were therefore obtained using a 5 m range. An additional motivation for this choice was that the sonar uses longer time (increase of approximately 30%) per circular scan when using a 10 m range compared with a 5 m range.

Note that, as our study investigated the effect of the introduction of a novel object into a fish population, the 'control distance' would be the distance between individual unhindered swimming fish. Since the naked sonar attached to its holder including a weight presents in itself an object which likely would affect the behaviour of the fish, it was not possible to collect comparative data in the absence of an intrusive object. Therefore, our study compared the effect of various objects to each other.

To summarise, Table 1 lists all the different trials conducted for shape, size and colour during P1, P2 and P3, including which cages and locations were used, and which impact factors the trials were used to

analyse.

2.2. Data processing

Since manually analysing the data collected with the Ping360 would be very difficult and time consuming, we developed a method for automatic processing of the data based on Machine Learning methods. Specifically, a Deep Learning (DL) semantic segmentation approach was adapted to automatically determine fish swimming patterns around the structure and then estimate the distances the fish avoided the structures. This section outlines how this method was adapted to our study, and how the datasets were prepared before the automated analyses.

2.2.1. Data preparation

2.2.1.1. Ping360 images and fish swimming patterns. Two sonars were used in all trials listed in Table 1, but since the bottom and top sonars provided similar results in all cases (see data excerpt in Appendix A, Fig. 10), we therefore assumed that the same distances are experienced at different depths of the intrusive object and analyses were limited to the data from the bottom sonar.

It took approximately 8 s for the single-beam Ping360 sonar to complete a circular scan when set to a range of 5 m. The raw sonar data from each scan are given as time-series arrays of intensity values reflecting echo strength in a Cartesian coordinate system. To make the data more intuitive, the raw data were represented in polar coordinates and converted into images providing a 360-degree view of the sonar's surroundings, as exemplified by Fig. 2(a).

Based on the findings of (Kruusmaa et al., 2020), it is likely that the propensity of salmon towards keeping a certain distance from structures observed in their proximity will induce circular swimming patterns around the structure. Such behaviour would appear as rings in the sonar images, and it is thus likely that the minimum distances the fish avoid the structures can be determined by finding the inner boundaries of the "fish school rings" (e.g., the closed red line in Fig. 2(a)). For convenience, in this article, we refer to the minimum distance fish keep away from the structure as fish avoidance distance to structure, denoted by d_{vpref}, and refer to the inner boundary of a "fish school ring" as a fish swimming pattern.

2.2.1.2. Cumulative Fish Presence (CFP) images. Due to the high variation in individual fish behaviours, fish swimming patterns around the structure may vary greatly over short periods of time. This makes determining fish avoidance distances from one-circular-scan images an inaccurate approach. To acquire a more robust approach, we derived sonar images called Cumulative Fish Presence (CFP) images that accumulated the data from all circular scans over 1-, 5-, and 10-min periods to determine fish avoidance distances around structures.

Sonar data typically contains stripe noises and structure signals that may be greatly emphasised when accumulated over time as when deriving CFP images. To compensate for this, the data used to derive 5- and 10-min CFP images was destriped prior to the conversion to polar coordinates by applying morphological closing with a rectangular-shaped structuring element of size 1×3 to the raw data array (Gonzalez and Woods, 2006). To further reduce the impact of such error sources, the 5- and 10-min CFP images were subjected to additional post-processing to produce higher quality images. This was done by conducting histogram equalisation on the CFP images to balance image intensity after their completion (Gonzalez and Woods, 2006). These pre- and post-processing procedures were not applied when generating 1-min CFP images since these were less affected by stripes and structure signals presented and since the preprocessing tended to weaken fish signals in the 1-min CFP images, resulting in inaccurate fish swimming patterns.

2.2.1.3. Invalid data. After the CFP image datasets had been derived from the collected data, we identified different types of CFP images that should be considered invalid as they were unlikely to yield useful outcomes when subjected to the DL method adapted in this study. Three different types of data (Fig. 3) were categorised as invalid, and the DL method was trained to filter out all CFP images matching these and not use them in the final analyses. The first type of invalid data was characterised by strong noise around the sonar that overrode fish signal as seen in Fig. 3(a). Noise reduction methods such as reducing the intensity of potential noise pixels detected by Otsu's method (Otsu, 1979) were investigated. Although this improved some datasets, the noise around the sonar was too strong to be effectively reduced in other cases. In the second type of invalid data identified in this study (Fig. 3(b)), the fish swimming pattern covered less than a semicircle. Although such data may sometimes be representative of the actual fish response and distribution, the resulting distance estimates from the DL-method were considered more uncertain and less conclusive than when based on data showing a ring shaped distribution. The third type of invalid data was mainly one-circular-scan images, showing very few fish swimming around the structures (Fig. 3(c)). While this type of invalid data was not common in CFP images, they were used as additional training data to

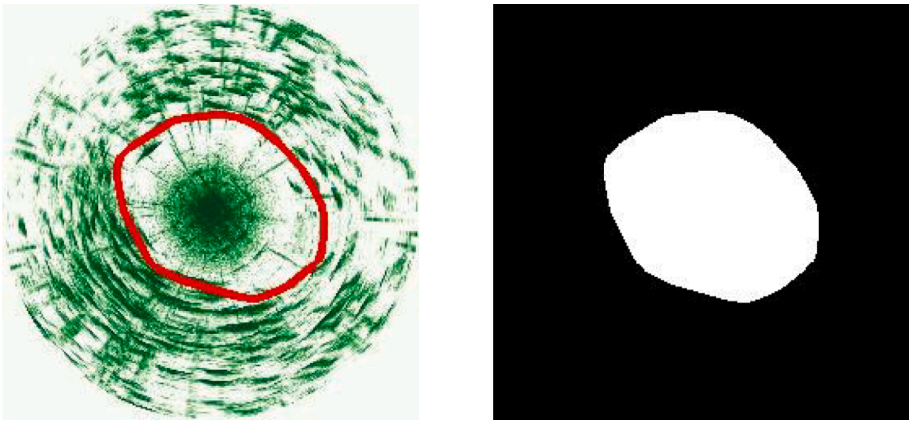

(a) (b)

Fig. 2. (a) One-circular-scan sonar image of fish around the structure. Green scale intensities represent reflections from fish and other objects, the red line represents the boundary of the fish swimming pattern; (b) Annotation mask of fish swimming pattern. (For interpretation of the references to colour in this figure legend, the reader is referred to the web version of this article.)

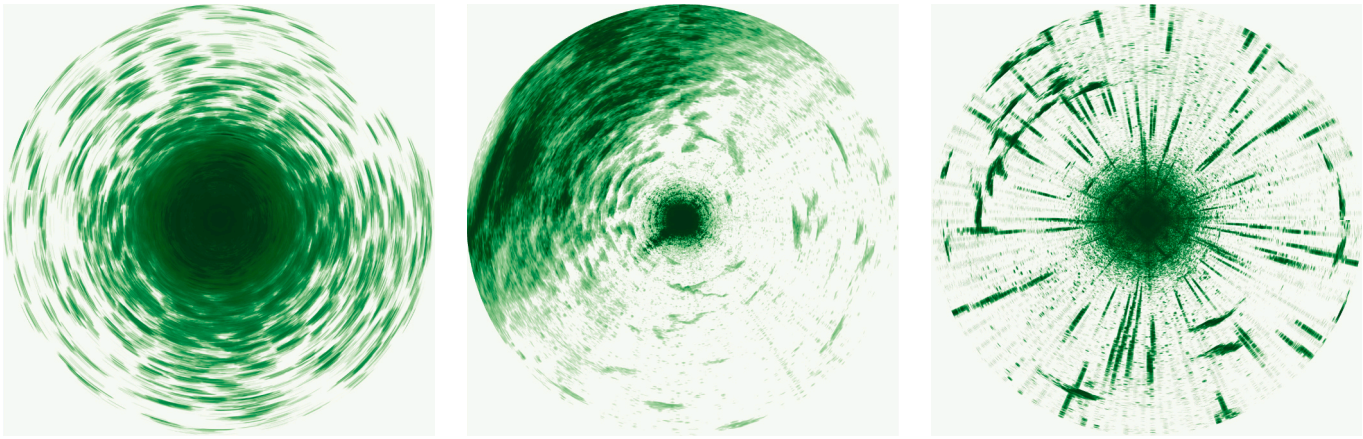

Fig. 3. Examples of invalid data. (a) The strong noise around the sonar overrides fish signal; (b) Fish swimming pattern is less than a semicircle; (c) Too few fish within range.

increase the diversity of the training data to obtain a more robust DL model.

2.2.1.4. Deep Learning (DL) method for automatic recognition of fish swimming patterns. The first step in developing the DL model was to create a dataset of annotate CFP images suitable for training, validating and testing the model. We obtained >4000 CPF images (1-, 5- and 10-min) and 10% of them (150, 108 and 150 images, respectively) were randomly selected for training. As the 5-min images were generally similar to the 10-min ones, we reduced the number of 5-min images used for training in order to increase balance in the training dataset. In addition, 120 one-circular-scan images were used to increase the diversity of the training dataset. These non-cumulative images were not analysed in the present study. The images were then annotated by labeling the images with solid white polygons covering the areas devoid of fish (indicating that they avoided the structures) in the sonar data. A binary mask denoting the inner boundary of the covered region was then derived, as shown in Fig. 2(b). Solid-filled polygons were used here instead of closed curves because they have more foreground pixels than curves which helps balance positive and negative samples in the dataset, thereby making it easier to train a model with good performance. <10% of all CFP images were categorised as invalid data according to the previously mentioned criteria, and were annotated by solid black masks to indicate that they should not be used in further analyses. The resulting annotated dataset was randomly split into 80% for training, 10% for validation, and 10% for testing.

2.2.1.5. Deep learning model. Several state-of-art (SoA) DL semantic segmentation models, such as FCNs (Long et al., 2015), SegNet (Badrinarayanan et al., 2017), and U-Net (Ronneberger et al., 2015), were implemented on a common platform (NVIDIA RTX A2000 GPU with 4 GB of memory), trained using the CFP datasets and evaluated with respect to their ability to segment out the desired fish swimming patterns. The best segmentation results were obtained with a U-Net++ model (Zhou et al., 2020), trained with Adam optimisation with a learning rate of 0.0001 as the optimizer, binary cross entropy as the loss, batch size of 4, and early stopping patience of 10.

U-Net++ is a symmetric U-shaped encoder-decoder neural network architecture with additional skip connections (Ronneberger et al., 2015; Zhou et al., 2018, 2020). The encoder part in the network acts as a feature extractor that extracts multiple feature maps of different scales from the input image. It consists of convolution blocks followed by a max-pooling down-sampling, where the convolution block used in our model has two convolutions with a kernel size 3 × 3, each followed by a Rectified Linear Unit (ReLU). The decoder part in the network is used to restore the spatial resolutions of the feature maps corresponding to the feature map resolutions from encoder, and it consists of up-sampling operations followed by a convolution block. The skip connections between the encoder and decoder aim to concatenate the low-level features (extracted from the encoder) with the corresponding high-level features (obtained from the decoder) to recover the spatial information lost during the max-pooling operations. In U-Net++, a series of nested dense convolution blocks (Huang et al., 2017) are used on the skip pathways to better bridge the semantic gap between encoder and decoder feature maps prior to concatenation. Furthermore, this design of skip connections allows U-Net++ to generate multiple full-resolution feature maps at different semantic scales (i.e., $X^{0,1}$, $X^{0,2}$, $X^{0,3}$, and $X^{0,4}$), so that only one loss layer is needed to determine the optimal depth of the network. At the last layer of U-Net++, a 1 × 1 convolution followed by a pixelwise softmax activation is applied to the full-resolution feature map to create a mask with the same resolution as the input image for semantic segmentation. Fig. 4 presents the architecture of U-Net++ we used for fish swimming pattern recognition.

2.2.1.6. Fish avoidance distance estimation. The DL-based method was then applied to the >4200 valid CFP images obtained in the study, outputting a binary image for each input CFP image. These were similar to Fig. 2(b), where the white region corresponds to the area without fish based on their avoidance of the structure as identified by the U-Net++ model. By then tracing the one-pixel-wide contour of the white region (Gonzalez and Woods, 2006), a curve delimiting the fish swimming pattern was obtained. The avoidance distance of the fish towards the intrusive structure was then found by averaging the distance from each pixel on the fish swimming pattern curve to the structure/image centre (Fig. 5 illustrates this process). To determine the avoidance distances for each impact factor, we used the cases where the sonar data had least interfering signals, and was thus most likely to yield consistent results. The findings obtained were validated with the remaining sonar data for each case. All three accumulation intervals (i.e., 1-, 5- and 10-min) were included in the analyses, as short-term cumulative measurements will contain data from fewer fish and thus probably reveal more about individual fish response, while long-term cumulative measurements are more likely to reflect group responses and were considered more robust than 1- and 5-min estimates.

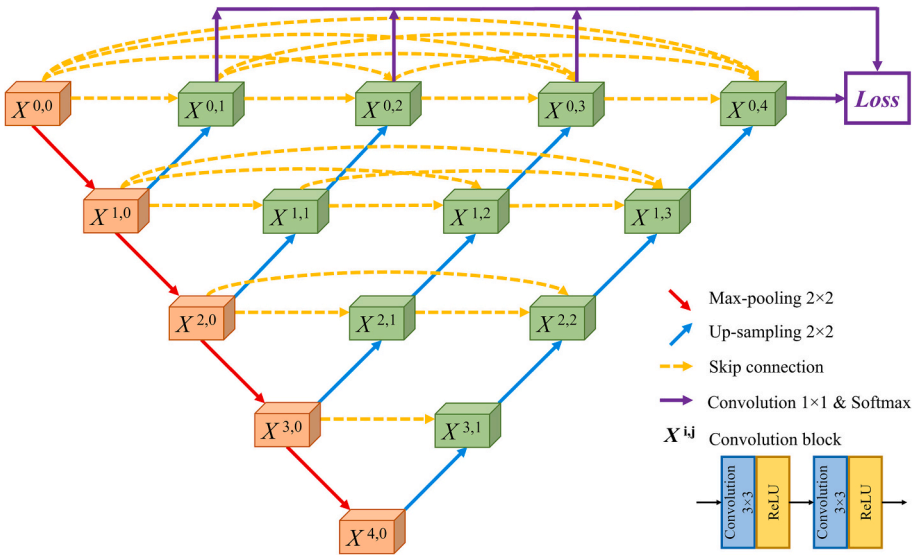

Fig. 4. U-Net++ architecture.

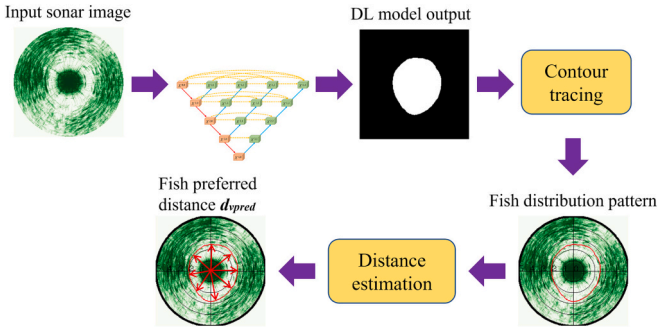

Fig. 5. Fish avoidance distance estimation process.

3. Results

The DL-based method was applied to the datasets from all case studies, resulting in statistical distributions describing the fish avoidance distance determined for each of the cases.

Collective information and fish avoidance distance estimation statistics for each case can be found in Appendix A. Tables 2 and 3 summarise the results for structure appearance factors and fish weights, respectively. As expected, variability decreased with increased accumulation time when analysed for the impacts of size, shape and colour (Fig. 6). Since we were primarily interested in generic rather than individual-specific responses, the 10-min values were used in the analyses presented in the following subsections.

3.1. Impact of structure shape and size

The avoidance distance estimates show that, for white structures (Fig. 6(a)), the fish kept the shortest distance from the small cylinder (0.64 m), followed by the big cylinder (0.82 m) and the cube (0.89 m), indicating that avoidance distance increased from small to big cylinder (21%), and from big cylinder to cube (9%). The pattern was similar for yellow structures (Fig. 6(b)), with the fish keeping closer to the small cylinder (0.90 m) than both the cube (1.39 m) and the big cylinder (1.43 m). In relative terms, this implied a larger increase (37%) from small to big cylinder, while the difference between big cylinder and cube was negligible (3%). In summary, the results (Fig. 6) show that the distance of fish from the object increased with the size of the objects, but was independent of the object's shape.

3.2. Impact of structure colour

Comparing the results from the white and yellow objects (Fig. 6) showed that the fish stayed generally closer to the white structures (max. distance <0.9 m) than the yellow ones (min. distance 0.9 m). This equaled a 50% larger distance to yellow shapes.

3.3. Impact of fish weight

To investigate if fish weight had an impact on the distance kept to a structure, we compared data from trials using the yellow cube structure conducted with fish of different sizes, including fish weighing 1 kg, 2.5 kg and 5 kg (Table 3). The results show a linear relationship between avoidance distance and fish weight, with larger fish keeping a larger distance from the object (Fig. 7).

Table 2
Comparison of results of avoidance distance for structure appearance impact investigation based on accumulation times of 1 min, 5 mins and 10 mins collected from Cage 12 (P3) with a fish weight of 1.084 kg, population size of 172,563, and a structure depth of 8 m.

Case		Mean ± Standard deviation [m]			Minimum [m]			Maximum [m]		
		1 min	5 mins	10 mins	1 min	5 mins	10 mins	1 min	5 mins	10 mins
Big Cylinder	White	0.93 ± 0.06	0.82 ± 0.02	0.82 ± 0.01	0.85	0.79	0.80	1.10	0.85	0.83
	Yellow	1.72 ± 0.21	1.47 ± 0.09	1.43 ± 0.06	1.34	1.37	1.37	2.14	1.69	1.53
Cube	White	0.99 ± 0.04	0.90 ± 0.01	0.89 ± 0.01	0.90	0.87	0.88	1.13	0.92	0.90
	Yellow	1.72 ± 0.26	1.44 ± 0.17	1.39 ± 0.13	1.12	1.13	1.20	2.43	1.68	1.58
Small Cylinder	White	0.77 ± 0.05	0.65 ± 0.03	0.64 ± 0.02	0.68	0.60	0.61	0.98	0.69	0.67
	Yellow	1.23 ± 0.25	0.92 ± 0.09	0.90 ± 0.07	0.831	0.79	0.80	1.90	1.150	1.01

Table 3
Results of avoidance distance for fish weight impact investigation based on reactions to the yellow cube.

Trials	Cage	Fish weight [kg]	Fish population	Mean ± Standard deviation [m]			Minimum [m]			Maximum [m]		
				1 min	5 mins	10 mins	1 min	5 mins	10 mins	1 min	5 mins	10 mins
P3	12	1.0	172,000	1.71 ± 0.26	1.44 ± 0.17	1.39 ± 0.13	1.12	1.12	1.20	2.43	1.68	1.58
P3	14	1.0	175,000	2.45 ± 0.18	2.10 ± 0.18	2.03 ± 0.13	2.06	1.90	1.88	2.85	2.44	2.22
P1	1	2.5	195,000	2.15 ± 0.27	1.97 ± 0.25	1.88 ± 0.12	1.71	1.68	1.69	3.27	2.93	2.07
P1	8	2.6	180,000	2.17 ± 0.26	1.93 ± 0.15	1.89 ± 0.12	1.73	1.74	1.75	3.15	2.34	2.18
P2	1	5.0	99,000	3.39 ± 0.25	2.99 ± 0.16	2.92 ± 0.14	2.87	2.71	2.73	3.92	3.15	3.12

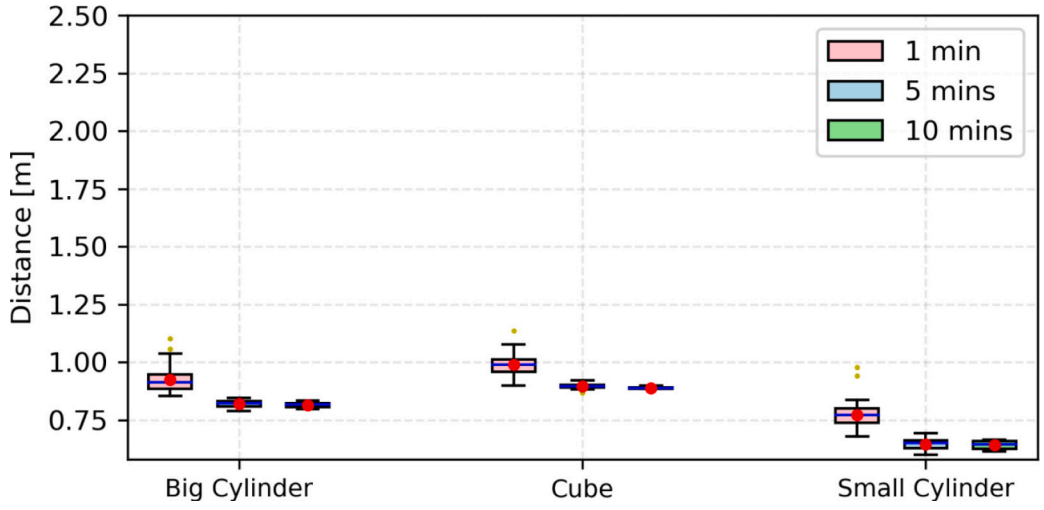

(a)

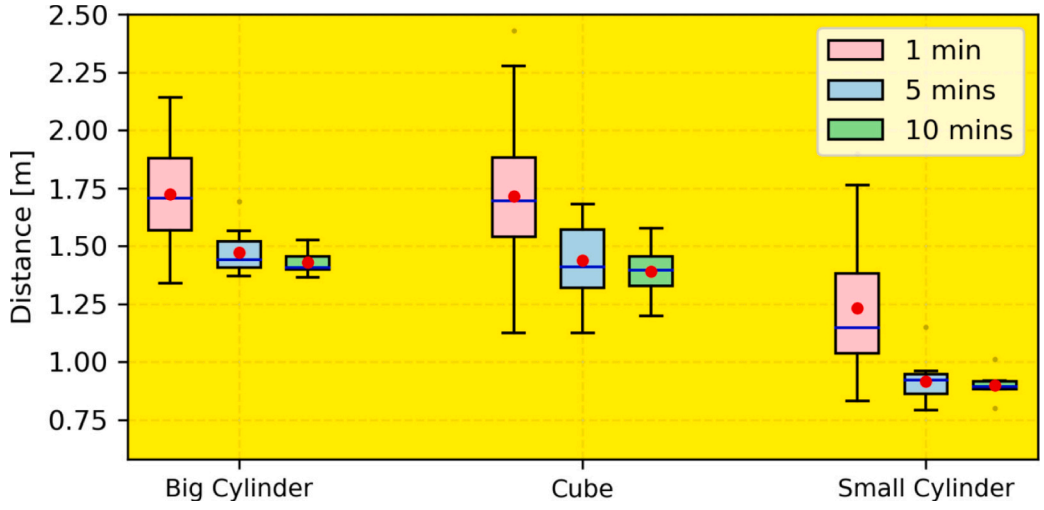

(b)

Fig. 6. Fish responses to structures of different shape, size, and colour collected from Cage 12 in P3, showing boxplots featuring the minimum, first quartile, mean (red dot), median (blue horizontal line), third quartile, maximum and outliers (yellow dot) for 1-, 5- and 10-min CFPs for (a) white structures and (b)yellow structures. (For interpretation of the references to colour in this figure legend, the reader is referred to the web version of this article.)

3.4. Cage effects

To explore whether fish in two different cages respond similar to the same object, we compared the results obtained in Cages 12 and 14 at Korsneset in 2022 (Table 1). The data from the two cages show similar trends in that both fish groups stayed further from large cylinders and cubes than from small cylinders, and in general kept greater distances from yellow than from white structures (Fig. 8). However, the fish in Cage 14 kept greater distances from all structures than the fish in Cage 12 (cube: white 11% and yellow 43% greater in Cage 14, big cylinder: white 16% and yellow 28% greater, small cylinder: white 45% greater, no data in Cage 14 for yellow). Interestingly, the data on white

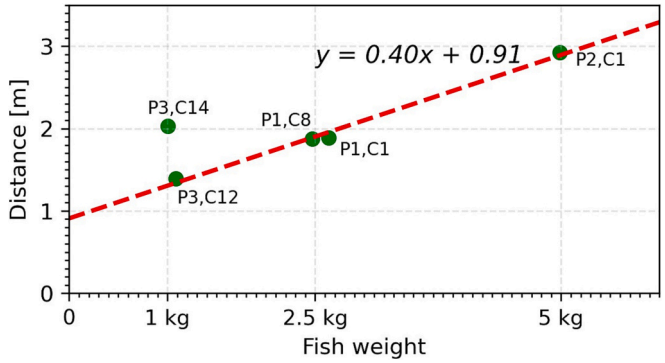

Fig. 7. Linear regression of the means of 10-min estimates for the distance kept by fish in different size classes from the yellow cube. $R^2 = 0.993$, $P = 0.004$. (For interpretation of the references to colour in this figure legend, the reader is referred to the web version of this article.)

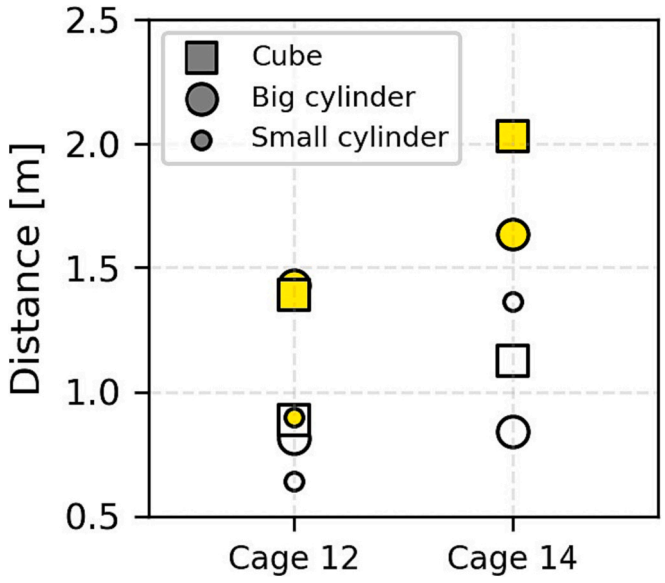

Fig. 8. Means of 10-min estimates for Cage 12 and Cage 14. The data were collected from the bottom sonar in Cage 12 and 14 in P3, respectively.

structures from Cage 14 implies that the fish stayed further from the small cylinder than from the big cylinder and the cube, which is unlike the pattern seen in Cage 12.

4. Discussion

This study successfully measured differences in fish response around structures of variable shape, size, and colour using a novel Machine Learning method for fish avoidance distance studies adapting a Deep Learning (DL) semantic segmentation approach to automatically determine fish swimming patterns around a structure. Such methods have been extensively investigated in other domains and it is the first time such an approach was adapted to systematic studies in aquaculture. By applying the DL-method upon sonar data, several fish responses towards structures in a sea-cage were identified and quantified as summarized and categorised in Table 4. The method can be extended to target fish responses to other impact factors than those explored here, and can be applied to the studies targeting the responses of different species and other segments than aquaculture (e.g., fisheries, conservation).

Previous studies have indicated that the size and colour of an intrusive object are important factors in determining how fish respond to this object (Marras and Porfiri, 2012; Kruusmaa et al., 2020). While these pioneering studies described the holistic responses towards such objects, our study complements their findings by exploring the specific reactions are elicited by the various features of such objects. Our results thus both confirm these findings, and add more knowledge in demonstrating a clear/direct link between structure size and fish response, as the fish stayed closer to smaller structures than to bigger ones in all experimental setups. In addition, fish maintained shorter distances from white structures than from yellow structures of similar shape and size. Similar to the findings of (Kruusmaa et al., 2020) and (Marras and Porfiri, 2012), this implies that colour might affect how fish respond to a structure. There was, however, no clear evidence of preference towards cylindrical or cubic shapes, indicating that the shape of the structure might be not an important factor affecting the fish response.

Table 4
Fish responses related to different structures.

Impact factor	Reaction
Shape	Unclear
Size	Greater distance to larger objects
Colour	Greater distance to yellow than to white objects
Fish weight (kg)	Average distance of 3.8 body length (resulting in larger fish keeping a larger actual distance)

The comparison across fish weights concluded that fish weight had an impact on the avoidance distance, with bigger fish tending to stay farther from structures than smaller fish. Interestingly, there was a nearly linear relationship between avoidance distance and fish weight. To explore this further, we used weight-length data obtained from a commercial farming site (Fig. 11 in Appendix A) to derive estimated body lengths (BL, i.e., the length of the individual fish) for the three fish weights used in the present study (1.0 kg: 0.44 m; 2.5 kg: 0.55; 5.0 kg: 0.73 m, Table 8 in Appendix A). This resulted in a average avoidance distance of 3.8 BL across fish weights (1 kg: 3.9 BL, 2.5 kg: 3.4 BL, 5 kg: 4.0 BL). This narrow range of values implies that there might be a strong relationship between the length of an individual fish and the avoidance length it tends to keep to invasive objects. Based on this, it is possible that a scalar number (or narrow range of scalar numbers) can be used together with fish length to estimate the distance fish in a farming situation would keep to invasive objects. This could in turn be useful when designing new vehicles or operations for use in aquaculture such that they have minimal impact upon the fish. However, as the fish in the three weight groups originated from three different genetic strains, it cannot be excluded that it is not fish size but genetic origin that is responsible for the variation in distance measured between the three groups. Ideally, future experiments should reassess the same fish group at different times during their growth phase to determine the true cause for the observed scalar relationship before it can be implemented as a design parameter for future vehicle and operation development.

While fish reactions to object shape, size and colour were consistent between cages, the direct comparison between fish from two cages showed consistent differences in distance to the objects. However, a closer scrutiny of the CFP images used in the analyses revealed that much of the data from the cases with the yellow cube, and white and yellow small cylinder for Cage 14 were characterised by the fish being only on one side of sonars, and further away from the structures than usual when they exhibit annular distributions around the object. These cases were as such close to being labelled as invalid data according to the previously mentioned criteria (see example in Fig. 9), which probably renders the data less suitable for concluding with regards to the existence of potential cage effects. This phenomenon may have arisen due to differences in the cage environment (e.g., current exposure, water quality) of Cages 12 and 14, which could influence the fish avoidance distance. To finally conclude on possible cage effects will require further experiments comparing more than two cages while keeping external factors as similar as possible.

Colours attenuate in seawater with depth, with red colours being lost

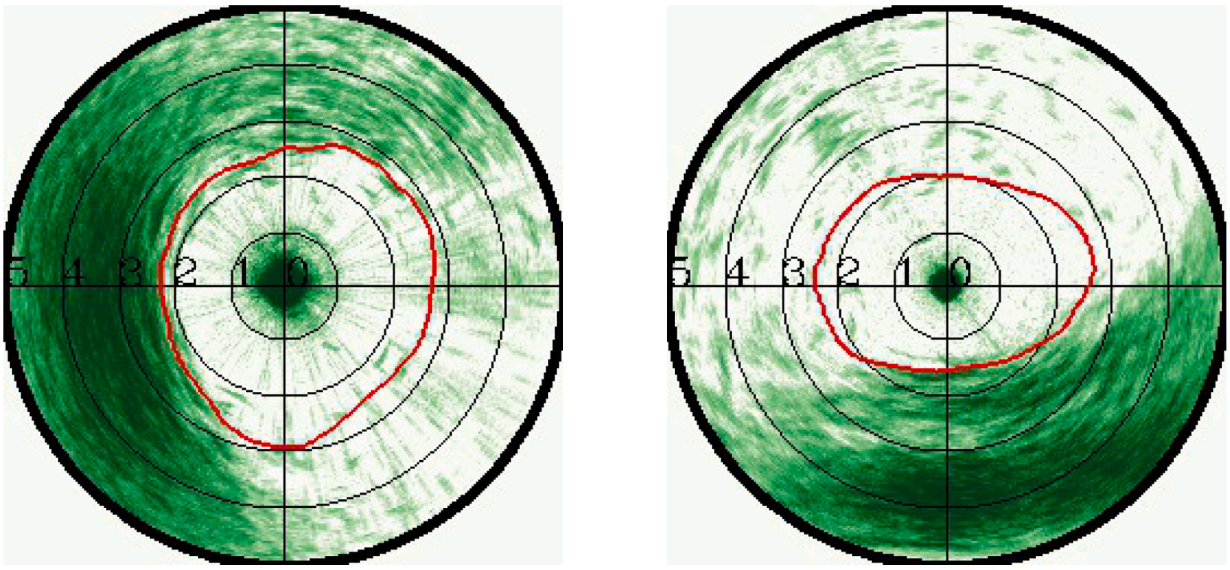

Fig. 9. The swimming patterns of the fish in Cage 14 for (a) the yellow cube and (b) the small white cylinder. (For interpretation of the references to colour in this figure legend, the reader is referred to the web version of this article.)

first, followed by orange and yellow (Pope and Fry, 1997)(for visualisation see e.g., (Carothers, NOAA-OE, n.d.)). The intensity of attenuation depends strongly on available light, as well as the presence of disturbing factors such as scattering particles or waves. As light intensity in the experimental depth was not measured, the amount of attenuation during the trials is unknown. The observed difference in reaction between the yellow and white structure imply that it was still visible. However, for a potential extension of the current study to investigate the effects of depth and light conditions on how fish perceive colour, inclusion of light penetration measurements is recommended. As colour vision in anadromous fish has capacity for change (e.g., connected to life cycle stages to allow adaptation to changing water properties in rivers vs. sea water) (Carleton et al., 2020); it cannot be excluded that fish of different age or originating from different genetic strains may display variation in their preference towards coloured objects. While it is possible that also the reaction towards shape or size is age or genetic strain related, the observed correlation of preferred distance to body length indicates a consistency with age. Differences between genetic populations could be the topic of further studies.

An initial study suggested strong currents and powerful waves can impact the swimming capabilities of fish (Hvas et al., 2021). Circular swimming of the fish in the cage will be abolished when current conditions exceed fish's preferred swimming speed. But shorter periods (hours) with current conditions above the preferred swimming speed would likely have negligible effects on fish (Hvas et al., 2021). Since health and safety concerns prevent conduction of experiments during adverse weather, including too strong currents, data collection was limited to days where fish are expected to have experienced benign conditions. Moreover, since we focused on local fish distribution around the intrusive object in this study and only observed the radial distance fish kept from the intrusive object, currents and waves are unlikely to have a significant impact on our outcomes.

Due to practicalities, it was not possible to conduct our studies using real more replicate cages for each trial. Having proper more replicates on cage level would strengthen our findings and the likelihood that they reflect the real dynamics between fish and intrusive objects in sea-cages. However, >170,000 fish per cage allowed the assumption that a given group of fish encountered the object only once during the up to six replicate measurements in a cage, providing a robust measurement for each cage. Moreover, the data collected and analysed in this work was found sufficient to demonstrate the efficacy of the developed model and the drawing of initial conclusions. In the future, a similar setup and methods can be utilized for a more extensive study in more cages.

Sensors, robots/UUVs and other technological tools dedicated to aquaculture applications should strive to minimise the disturbance they induce upon the fish, while still being effective at their intended purpose. Our results provide new knowledge and insight into how farmed salmon respond towards obtrusive structures in the cage volume, covering a range of parameters related to the size and appearance of the structure. As such, our results are valuable inputs for the future design and development of such systems. However, it is important to note that we only addressed the impact of static parameters (i.e., shape, size, colour, fish weight). Therefore, to design systems fully suited for aquaculture purposes, similar studies should be aimed at the effects of dynamic parameters such as sound, lights and movements as these are other key factors during operations, particularly for robots/UUVs. This is work that could be achieved using the same instruments and ML-based approach as the method used in the present study.

Since our results quantify responses towards specific factors, they can also be used to derive mathematical representations of how salmon relate to objectives. These could then be used to expand existing models of salmon behaviour (Føre et al., 2009, 2014; Føre et al., 2016) to yield a more complete representation of the behavioural dynamics in salmon sea-cages. This could be beneficial both for providing an arena for virtually testing and refining vehicle designs in silico before physical protoyping, and for the future realisation of full digital twin technologies (Rasheed et al., 2020) for aquaculture.

Our method and results can thus through several different avenues, provide the insight and tools needed to develop solutions that help minimise the impact of adapted technologies on living fish in complex and dynamically changing environments, and thus contribute to improving the ethical sustainability, efficiency, and profitability of the aquaculture industry.

While our ML-method proved efficient at providing concrete measures of the fishes' avoidance distance to the objects, it has some shortcomings that could potentially render the use of the method

challenging. One such challenge is the use of solid black masks to mark the invalid datasets for the training of the DL-network. While this gave good results in terms of the method's ability to identify two of the invalid datatypes (Fig. 3(a) and (b)), it proved less effective at training for identifying the third type of invalid data (Fig. 3(c)). This might be because there are few fish in these images, which is diametrically opposite to the case implied to the network when using solid black masks (i.e., that fish cover the entire image). One method of improving upon this could be to alter the data used to train for detecting such cases to a solid white disk covering the area scanned by the sonar, as this is more similar to the real situation, which is that there are few fish within sonar range.

Another potential source of inaccuracy is the assumption that the fish always form circular swimming patterns around the structures. This was true in almost all the CFD-images considered valid in our study, and might be true for most static cases where the object is not placed close to a second structure, such as the cage wall. However, when a structure (or vehicle) is in an operational state or otherwise exhibits dynamics such as sound and light, the distribution could become more asymmetric as the impact factors (e.g., movement, light) can then have a specific directivity. This implies that further development of the method should take more CFD-shapes into account during training to ensure robustness towards more dynamic conditions. One way of doing this would be to include images displaying other swimming patterns in the training process. A challenge there could be to identify such datasets, but it is likely that more such data would appear in experiments where the object or structure disturbing the fish exhibits dynamics.

5. Conclusions and future work

In this paper, we have developed a DL-based sonar data processing method to identify and quantify responses of fish under different impact factors during fish farm operations. The method has been successfully applied to relevant sonar data collected from the field trials to study fish avoidance distance in reaction to structures with varying shape, size, and colour. The results from our fish avoidance distance studies show that: fish responded to structure size, but did not distinguish between shapes; the larger the object, the greater the distance the fish kept from it, implying that larger objects have a greater impact on fish than small objects. Moreover, fish stayed further away from yellow than from white structures, regardless of shape or size, implying that yellow is a more visible and/or threatening colour than white. Finally, independent of fish weight, fish kept a distance of an average 3.8 body lengths to objects, while the actual avoidance distance is increasing with increasing fish weight.

For future work, in addition to avoidance distance, which is an important fish behaviour indicator that can be observed by sonar, more fish behaviours that cannot be observed by sonars, such as change of swimming direction and distance between fish, etc., will be explored by analysing the video data using computer vision methods (Saad et al., 2023). The quantified parameters of fish behaviour will be used to extend the existing mathematical models of Atlantic salmon behaviour in sea-cages (Føre et al., 2009) to mimic the observed responses of farmed fish. This will critically improve autonomous operations in fish farms, reduce potential negative impacts on fish during complex operations, as well as improve fish welfare by moderately adding extra stimuli that may have positive impacts on fish. In addition, more studies will be conducted to identify and quantify fish responses to more dynamic stimuli such as depth, light, sound and movements.

CRediT authorship contribution statement

Qin Zhang: Formal analysis, Methodology, Writing – original draft, Conceptualization, Software. **Nina Bloecher:** Conceptualization, Writing – review & editing, Methodology. **Linn Danielsen Evjemo:** Resources, Writing – review & editing. **Martin Føre:** Conceptualization, Writing – review & editing. **Biao Su:** Methodology, Writing – review & editing. **Espen Eilertsen:** Data curation, Resources. **Mats Aarsland Mulelid:** Data curation, Visualization, Resources. **Eleni Kelasidi:** Data curation, Methodology, Resources, Conceptualization, Funding acquisition, Project administration, Writing – original draft.

Declaration of Competing Interest

The authors declare the following financial interests/personal relationships which may be considered as potential competing interests:

Eleni Kelasidi reports financial support was provided by Research Council of Norway.

Data availability

The authors do not have permission to share data.

Acknowledgments

The work presented in this publication is supported by the Research Council of Norway (RCN) project CHANGE (RCN project no. 313737). We also thank Dr. Pascal Klebert at SINTEF Ocean for providing the data used to derive the weight/length relationship for salmon used to find distances in body lengths.

Appendix A

The appendix provides a supplementary figure comparing top and bottom sonars, lists the case information for the field trials in P1, P2, and P3, along with fish avoidance distance estimation statistics, and provides figures and tables used to derive the length-weight relationship for farmed salmon

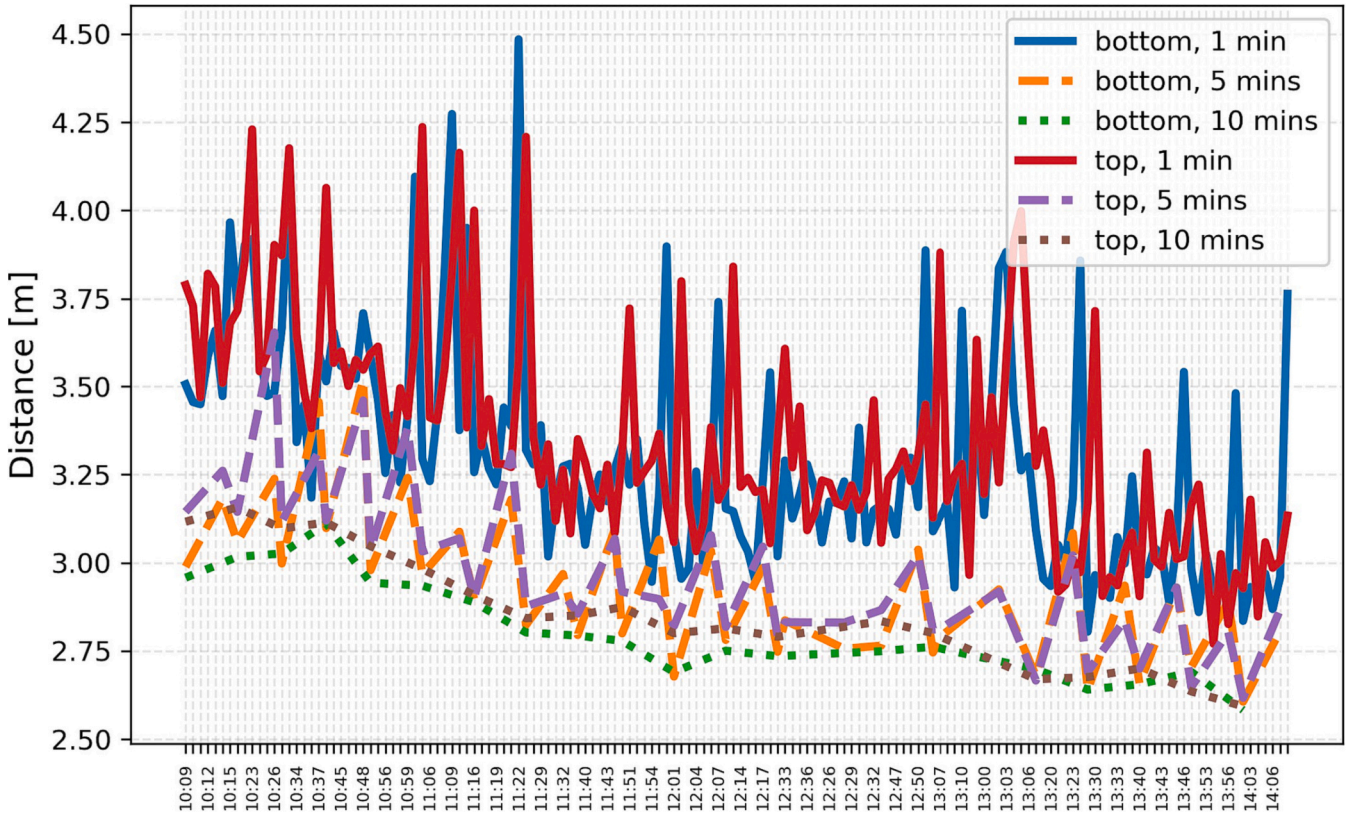

Fig. 10. Time-series curves of fish avoidance distances estimated from bottom and top sonar data, where *x*-axis presents the start times of CFP images and *y*-axis presents the estimated fish avoidance distances.

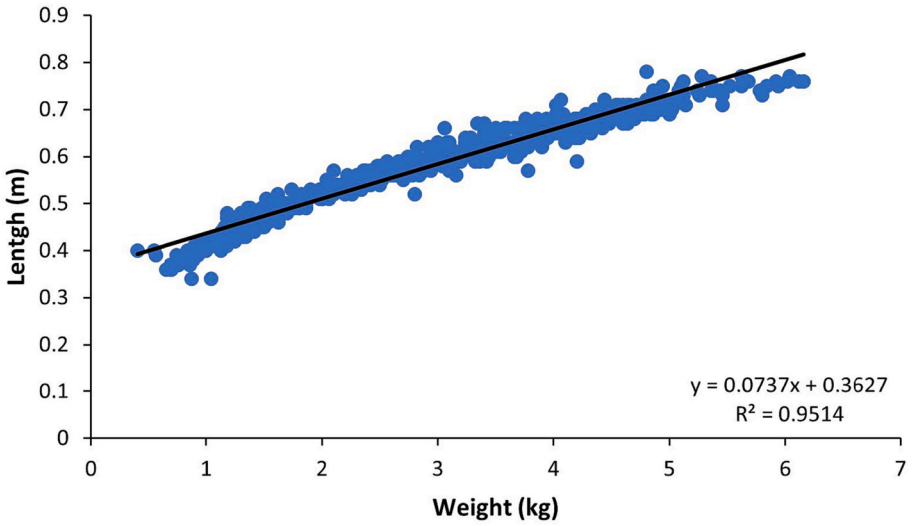

Fig. 11. Linear regression for weight to length ratio based on measurements taken from 630 fish from 3 cages during the growth season 2021/2022 at an ACE farm site (Pascal Klebert, unpublished data).

Table 5
Fish avoidance distance estimates from 1-min CFPs.

Trials	Case	Date	Cage	Fish weight [kg]	Fish population	Depth	Sonar range	Mean ± Standard deviation [m]		Minimum [m]		Maximum [m]	
								Bottom	Top	Bottom	Top	Bottom	Top

(*continued on next page*)

Table 5 (*continued*)

Trials	Case		Date	Cage	Fish weight [kg]	Fish population	Depth	Sonar range	Mean ± Standard deviation [m]		Minimum [m]		Maximum [m]	
									Bottom	Top	Bottom	Top	Bottom	Top
P1*	Cube	Yellow	16-Jun	1	2.469	195,832	8	5	2.15 ±0.27	2.23 ±0.19	1.71	1.90	3.27	3.00
			17-Jun	8	2.638	180,037	8	5	2.17 ±0.26	2.18 ±0.19	1.73	1.61	3.15	2.97
P2*	Cube	Yellow	18-Oct	1	4.989	99,243	8	5	3.39 ±0.25	3.09 ±0.16	2.87	2.74	3.92	3.32
	Big Cylinder	White	5-Sep	12	1.084	172,563	8	5	0.93 ±0.06	1.01 ±0.10**	0.85	0.91**	1.10	1.58**
			5-Sep	14	1.004	175,034	8	5	0.97 ±0.12	1.05 ±0.09**	0.84	0.98**	1.64	1.57**
	Big Cylinder	Yellow	6-Sep	12	1.084	172,563	8	5	1.72 ±0.21	1.21 ±0.07**	1.34	1.10**	2.14	1.43**
			6-Sep	14	1.004	175,034	8	5	1.96 ±0.16	1.18 ±0.06**	1.63	1.13**	2.27	1.56**
	Cube	White	6-Sep	14	1.004	175,034	8	5	1.54 ±0.25	1.81 ±0.30**	1.10	1.24**	1.96	2.45**
			7-Sep	12	1.084	172,563	8	5	0.99 ±0.04	1.10 ±0.05**	0.90	0.99**	1.13	1.24**
P3														
	Cube	Yellow	7-Sep	12	1.084	172,563	8	5	1.71 ±0.26	1.78 ±0.29	1.12	1.15	2.43	2.50
			7-Sep	14	1.004	175,034	8	5	2.45 ±0.18	2.72 ±0.22	2.06	2.24	2.85	3.17
	Small Cylinder	White	7-Sep	14	1.004	175,034	8	5	2.05 ±0.26	2.12 ±0.22	1.72	1.67	2.60	2.46
			8-Sep	12	1.084	172,563	8	5	0.773 ±0.051	0.85 ±0.06	0.68	0.76	0.98	1.10
	Small Cylinder	Yellow	8-Sep	12	1.084	172,563	8	5	1.23 ±0.25	1.44 ±0.27	0.83	1.02	1.90	2.30
			8-Sep	14	1.004	175,034	8	5	***	2.03 ±0.11	***	1.80	***	2.29

* The data for P1 and P2 were taken from the intervals between sound tests, from which the statistics on fish avoidance distances were derived.
** The raw data have strong noise around the sonar, an additional noise reducing step was performed when generating the CFP sonar images.
*** The bottom sonar encountered a timing issue that makes it impossible to extract data corresponding to the time of the tests.

Table 6
Fish avoidance distance estimates from 5-min CFPs.

Trials	Case		Date	Cage	Fish weight [kg]	Fish population	Depth	Sonar range	Mean ± Standard deviation [m]		Minimum [m]		Maximum [m]	
									Bottom	Top	Bottom	Top	Bottom	Top
P1*	Cube	Yellow	16-Jun	1	2.469	195,832	8	5	1.97 ±2.25	2.10±0.13	1.67	1.90	2.93	2.43
				8	2.638	180,037	8	5		2.07±0.15	1.74	1.87	2.34	2.58

(*continued on next page*)

Table 6 (*continued*)

Trials	Case		Date	Cage	Fish weight [kg]	Fish population	Depth	Sonar range	Mean ± Standard deviation [m]		Minimum [m]		Maximum [m]	
									Bottom	Top	Bottom	Top	Bottom	Top
			17-Jun						1.93 ±0.15					
P2*	Cube	Yellow	18-Oct	1	4.989	99,243	8	5	2.99 ±0.16	2.96±0.19	2.71	2.66	3.15	3.26
			5-Sep	12	1.084	172,563	8	5	0.82 ±0.02	0.93 ±0.02**	0.79	0.89**	0.85	0.95**
	Big Cylinder	White												
			5-Sep	14	1.004	175,034	8	5	0.84 ±0.03	0.99 ±0.03**	0.77	0.95**	0.88	1.03**
			6-Sep	12	1.084	172,563	8	5	1.47 ±0.09	1.10 ±0.06**	1.37	1.03**	1.69	1.20**
	Big Cylinder	Yellow												
			6-Sep	14	1.004	175,034	8	5	1.69 ±0.12	1.05 ±0.04**	1.51	1.01**	1.89	1.13**
			6-Sep	14	1.004	175,034	8	5	1.16 ±0.12	1.66 ±0.31**	0.99	1.29**	1.35	2.06**
	Cube	White												
			7-Sep	12	1.084	172,563	8	5	0.90 ±0.01	1.06 ±0.03**	0.87	1.02**	0.92	1.12**
P3														
			7-Sep	12	1.084	172,563	8	5	1.44 ±0.17	1.58±0.12	1.13	1.41	1.68	1.77
	Cube	Yellow												
			7-Sep	14	1.004	175,034	8	5	2.10 ±0.18	2.37±0.24	1.90	2.09	2.44	2.72
			7-Sep	14	1.004	175,034	8	5	1.50 ±0.19	1.83±0.16	1.35	1.60	1.77	2.00
	Small Cylinder	White												
			8-Sep	12	1.084	172,563	8	5	0.65 ±0.03	0.73±0.06	0.60	0.67	0.69	0.82
			8-Sep	12	1.084	172,563	8	5	0.92 ±0.09	1.17±0.11	0.79	1.03	1.15	1.39
	Small Cylinder	Yellow												
			8-Sep	14	1.004	175,034	8	5	***	1.66±0.06	***	1.59	***	1.71

* The data for P1 and P2 were taken from the intervals between sound tests, from which the statistics on fish avoidance distances were derived.
** The raw data have strong noise around the sonar, an additional noise reducing step was performed when generating the CFP sonar images.
*** The bottom sonar encountered a timing issue that makes it impossible to extract data corresponding to the time of the tests.

Table 7
Fish avoidance distance estimates from 10-min CFPs.

Trials	Case		Date	Cage	Fish weight [kg]	Fish population	Depth	Sonar range	Mean ± Standard deviation [m]		Minimum [m]		Maximum [m]	
									Bottom	Top	Bottom	Top	Bottom	Top
			16-Jun	1	2.469	195,832	8	5	1.88 ±0.12	2.07±0.11	1.69	1.92	2.07	2.26
P1*	Cube	Yellow												
			17-Jun	8	2.638	180,037	8	5	1.89 ±0.12	2.03±0.10	1.75	1.93	2.18	2.32
P2*														
	Cube	Yellow	18-Oct	1	4.989	99,243	8	5	2.92 ±0.14	2.92±0.21	2.73	2.67	3.12	3.25

(*continued on next page*)

Table 7 (*continued*)

Trials	Case		Date	Cage	Fish weight [kg]	Fish population	Depth	Sonar range	Mean ± Standard deviation [m]		Minimum [m]		Maximum [m]	
									Bottom	Top	Bottom	Top	Bottom	Top
			5-Sep	12	1.084	172,563	8	5	0.82 ±0.01	0.92 ±0.02**	0.80	0.89**	0.83	0.94**
	Big Cylinder	White												
			5-Sep	14	1.004	175,034	8	5	0.84 ±0.03	0.98 ±0.03**	0.80	0.93**	0.87	1.02**
			6-Sep	12	1.084	172,563	8	5	1.43 ±0.06	1.10 ±0.06**	1.37	1.02**	1.53	1.18**
	Big Cylinder	Yellow												
			6-Sep	14	1.004	175,034	8	5	1.64 ±0.12	1.04 ±0.04**	1.46	1.00**	1.77	1.11**
			6-Sep	14	1.004	175,034	8	5	1.13 ±0.12	1.58 ±0.40**	0.99	1.34**	1.30	2.04**
	Cube	White												
			7-Sep	12	1.084	172,563	8	5	0.89 ±0.01	1.06 ±0.02**	0.88	1.04**	0.90	1.09**
P3														
			7-Sep	12	1.084	172,563	8	5	1.39 ±0.13	1.49±0.13	1.20	1.31	1.58	1.65
	Cube	Yellow												
			7-Sep	14	1.004	175,034	8	5	2.03 ±0.13	2.28±0.21	1.88	2.07	2.22	2.56
			7-Sep	14	1.004	175,034	8	5	1.37 ±0.17	1.80±0.14	1.25	1.61	1.48	1.93
	Small Cylinder	White												
			8-Sep	12	1.084	172,563	8	5	0.64 ±0.02	0.72±0.03	0.61	0.70	0.67	0.76
			8-Sep	12	1.084	172,563	8	5	0.90 ±0.07	1.15±0.08	0.80	1.04	1.01	1.13
	Small Cylinder	Yellow												
			8-Sep	14	1.004	175,034	8	5	***	1.60±0.02	***	1.58	***	1.61

* The data for P1 and P2 were taken from the intervals between sound tests, from which the statistics on fish avoidance distances were derived.
** The raw data have strong noise around the sonar, an additional noise reducing step was performed when generating the CFP sonar images.
*** The bottom sonar encountered a timing issue that makes it impossible to extract data corresponding to the time of the tests.

Table 8
Body length equivalents for the distances calculated based on the linear regression results.

Weight (kg)	Body length (m)	Average distance (m)	Distance in body lengths
1.0	0.44	1.71	3.9
2.5	0.55	1.89	3.4
5.0	0.73	2.92	4.0
		Average	3.8

References

Badrinarayanan, V., Kendall, A., Cipolla, R., 2017. SegNet: a deep convolutional encoderdecoder architecture for image segmentation. IEEE Trans. Pattern Anal. Mach. Intell. 39, 2481–2495. https://doi.org/10.1109/TPAMI.2016.2644615.

Bjelland, H.V., Føre, M., Lader, P., Kristiansen, D., Holmen, I.M., Fredheim, A., Grøtli, E. I., Fathi, D.E., Oppedal, F., Utne, I.B., et al., 2015. Exposed aquaculture in Norway. In: OCEANS 2015-MTS/IEEE. IEEE, Washington, pp. 1–10.

Carleton, K.L., Escobar-Camacho, D., Stieb, S.M., Cortesi, F., Marshall, N.J., 2020. Seeing the rainbow: mechanisms underlying spectral sensitivity in teleost fishes. J. Exp. Biol. 223, jeb193334.

Carothers, K., NOAA-OE NOAA Ocean Explorer: Deep Scope Background n.d. https://oceanexplorer.noaa.gov/explorations/04deepscope/background/deeplight/media/diagram3.html. Accessed: 2023-10-03.

FAO, 2020. The state of world fisheries and aquaculture 2020. In: Sustainability in Action, Rome.

Fernö, A., Huse, I., Juell, J.E., Bjordal, A., 1995. Vertical distribution of Atlantic salmon (*Salmo solar* L.) in net pens: trade-off between surface light avoidance and food attraction. Aquaculture 132, 285–296.

Føre, M., Dempster, T., Alfredsen, J.A., Johansen, V., Johansson, D., 2009. Modelling of Atlantic salmon (*Salmo salar* L.) behaviour in sea-cages: a lagrangian approach. Aquaculture 288, 196–204. URL: https://www.cabdirect.org/cabdirect/abstract/20093279217.

Føre, M., Alfredsen, J.A., Gronningsater, A., 2011. Development of two telemetry-based systems for monitoring the feeding behaviour of Atlantic salmon (*Salmo salar* L.) in aquaculture sea-cages. Comput. Electron. Agric. 76, 240–251.

Føre, M., Dempster, T., Alfredsen, J.A., Oppedal, F., 2014. Modelling of Atlantic salmon (*Salmo salar* L.) behaviour in sea-cages: using artificial light to control swimming

depth. Aquaculture 388–391, 137–146. https://doi.org/10.1016/j.aquaculture.2013.01.027.
Føre, M., Alver, M., Alfredsen, J.A., Marafioti, G., Senneset, G., Birkevold, J., Willumsen, F.V., Lange, G., Espmark, A., Terjesen, B.F., 2016. Modelling growth performance and feeding behaviour of Atlantic salmon (*Salmo salar* L.) in commercial-size aquaculture net pens: model details and validation through full-scale experiments. Aquaculture 464, 268–278.
Føre, M., Frank, K., Norton, T., Svendsen, E., Alfredsen, J.A., Dempster, T., Eguiraun, H., Watson, W., Stahl, A., Sunde, L.M., Schellewald, C., Skøien, K.R., Alver, M.O., Berckmans, D., 2017. Precision fish farming: a new framework to improve production in aquaculture. Biosyst. Eng. https://doi.org/10.1016/j.biosystemseng.2017.10.014. URL: http://www.sciencedirect.com/science/article/pii/S1537511017304488.
Føre, M., Svendsen, E., Alfredsen, J.A., Uglem, I., Bloecher, N., Sveier, H., Sunde, L.M., Frank, K., 2018. Using acoustic telemetry to monitor the effects of crowding and delousing procedures on farmed Atlantic salmon (*Salmo salar*). Aquaculture 495, 757–765.
Fossen, T.I., 2011. Handbook of Marine Craft Hydrodynamics and Motion Control. John Wiley & Sons.
Fraser, N., Metcalfe, N., 1997. The costs of becoming nocturnal: feeding efficiency in relation to light intensity in juvenile Atlantic salmon. Funct. Ecol. 11, 385–391.
Gonzalez, R.C., Woods, R.E., 2006. Digital Image Processing, 3rd ed. Prentice Hall, USA.
Hawkins, A., Johnstone, A., 1978. The hearing of the atlantic salmon, *Salmo salar*. J. Fish Biol. 13, 655–673.
Huang, G., Liu, Z., Van Der Maaten, L., Weinberger, K.Q., 2017. Densely connected convolutional networks. In: 2017 IEEE Conference on Computer Vision and Pattern Recognition (CVPR). IEEE, pp. 2261–2269. https://doi.org/10.1109/CVPR.2017.243.
Hvas, M., Folkedal, O., Oppedal, F., 2021. Fish welfare in offshore salmon aquaculture. Rev. Aquac. 13, 836–852.
Juell, J.E., Fosseidengen, J.E., 2004. Use of artificial light to control swimming depth and fish density of Atlantic salmon (Salmo salar) in production cages. Aquaculture 233, 269–282.
Kelasidi, E., Svendsen, E., 2022. Robotics for sea-based fish farming. In: Zhang, Q. (Ed.), Encyclopedia of Smart Agriculture Technologies. Springer International Publishing, Cham, pp. 1–20. https://doi.org/10.1007/978-3-030-89123-7_202-1.
Kelasidi, E., Liljeback, P., Pettersen, K.Y., Gravdahl, J.T., 2016. Innovation in underwater robots: biologically inspired swimming snake robots. IEEE Robot. Automat. Mag. 23, 44–62.
Kelasidi, E., Liljeback, P., Pettersen, K.Y., Gravdahl, J.T., 2017. Integral line-of-sight guidance for path following control of underwater snake robots: theory and experiments. IEEE Trans. Robot. 33, 610–628.
Kruusmaa, M., Gkliva, R., Tuhtan, J., Tuvikene, A., Alfredsen, J.A., 2020. Salmon behavioural response to robots in an aquaculture sea cage. R. Soc. Open Sci. 7, 191220.
Kryvi, H., Totland, G., 1997. Fiskeanatomi. høyskoleforlaget as.
Long, J., Shelhamer, E., Darrell, T., 2015. Fully convolutional networks for semantic segmentation. In: Proceedings of the IEEE Conference on Computer Vision and Pattern Recognition (CVPR), pp. 3431–3440. https://doi.org/10.1109/CVPR.2015.7298965.
Magnhagen, C., Johansson, K., Sigray, P., 2017. Effects of motorboat noise on foraging behaviour in eurasian perch and roach: a field experiment. Mar. Ecol. Prog. Ser. 564, 115–125.
Marras, S., Porfiri, M., 2012. Fish and robots swimming together: attraction towards the robot demands biomimetic locomotion. J. R. Soc. Interface 9, 1856–1868.
Migaud, H., Cowan, M., Taylor, J., Ferguson, H.W., 2007. The effect of spectral composition and light intensity on melatonin, stress and retinal damage in post-smolt Atlantic salmon, *Salmo salar*. Aquaculture 270, 390–404.
Norwegian Directorate of Fisheries, 2021-05-27. Atlantic Salmon, Rainbow Trout and Trout – Grow Out Production. URL: https://www.fiskeridir.no/English/Aquaculture/Statistics/Total/_/attachment/download/76712525-86ab-4f09bf06-d2d18bd7a48f:a9c92ed3fa6a6beb265538eeefff6829912ad299/sta-totalt-5salg.xlsx.
Oppedal, F., Dempster, T., Stien, L.H., 2011. Environmental drivers of Atlantic salmon behaviour in sea-cages: a review. Aquaculture 311, 1–18. URL: http://www.sciencedirect.com/science/article/pii/S0044848610007933. https://doi.org/10.1016/j.aquaculture.2010.11.020.
Otsu, N., 1979. A threshold selection method from gray-level histograms. IEEE Trans. Syst. Man Cybern. 9, 62–66.
Oxman, D.S., Barnett-Johnson, R., Smith, M.E., Coffin, A., Miller, D.L., Josephson, R., Popper, A.N., 2007. The effect of vaterite deposition on sound reception, otolith morphology, and inner ear sensory epithelia in hatchery-reared Chinook salmon (*Oncorhynchus tshawytscha*). Can. J. Fish. Aquat. Sci. 64, 1469–1478.
Paull, L., Saeedi, S., Seto, M., Li, H., 2013. AUV navigation and localization: a review. IEEE J. Ocean. Eng. 39, 131–149.
Pieniazek, R.H., Mickle, M.F., Higgs, D.M., 2020. Comparative analysis of noise effects on wild and captive freshwater fish behaviour. Anim. Behav. 168, 129–135.
Pope, R.M., Fry, E.S., 1997. Absorption spectrum (380–700 nm) of pure water. II. Integrating cavity measurements. Appl. Opt. 36, 8710–8723.
Rasheed, A., San, O., Kvamsdal, T., 2020. Digital twin: values, challenges and enablers from a modeling perspective. IEEE Access 8, 21980–22012.
Ronneberger, O., Fischer, P., Brox, T., 2015. U-Net: Convolutional networks for biomedical image segmentation. In: Medical Image Computing and Computer-Assisted Intervention (MICCAI). Springer, pp. 234–241. https://doi.org/10.1007/978-3-319-24574-4_28.
Saad, A., Jakobsen, S., Bondø, M., Mulelid, M., Kelasidi, E., 2023. Stereoyolo+deepsort: A framework to track fish from underwater stereo camera in situ. In: Proceedings of SPIE, the 16th International Conference on Machine Vision (ICMV). SPIE.
SINTEF, 2023. SINTEF ACE. URL. https://www.sintef.no/en/all-laboratories/ace/.
Sverdrup-Thygeson, J., Kelasidi, E., Pettersen, K.Y., Gravdahl, J.T., 2017. The underwater swimming manipulator—a bioinspired solution for subsea operations. IEEE J. Ocean. Eng. 43, 402–417.
Zhou, Z., Rahman Siddiquee, M.M., Tajbakhsh, N., Liang, J., 2018. UNet++: a nested U-Net architecture for medical image segmentation. In: Deep Learning in Medical Image Analysis and Multimodal Learning for Clinical Decision Support. Springer, pp. 3–11. https://doi.org/10.1007/978-3-030-00889-5_1.
Zhou, Z., Siddiquee, M.M.R., Tajbakhsh, N., Liang, J., 2020. UNet++: redesigning skip connections to exploit multiscale features in image segmentation. IEEE Trans. Med. Imaging 39, 1856–1867. https://doi.org/10.1109/TMI.2019.2959609.